Forward-angle elastic and quasielastic proton-nucleon cross sections and analyzing powers at 0.8 GeV

M. L. Barlett, G. W. Hoffmann, J. A. McGill,* B. Hoistad,
L. Ray, R. W. Fergerson, E. C. Milner, and J. A. Marshall
Department of Physics, The University of Texas at Austin, Austin, Texas 78712

J. F. Amann, B. E. Bonner, and J. B. McClelland
Los Alamos National Laboratory, Los Alamos, New Mexico 87545

G. S. Blanpied
Department of Physics, University of South Carolina, Columbia, South Carolina 29208

R. A. Arndt
Department of Physics, Virginia Polytechnic Institute and State University, Blacksburg, Virginia 24060
(Received 13 July 1982)

Using a liquid deuterium target, 800 MeV quasielastic $\vec{p}+n$ and $\vec{p}+p$ analyzing powers were measured over the center-of-momentum angular range 14°–75°. Elastic $\vec{p}+p$ analyzing powers were measured over the center-of-momentum angular range 10°–47° using a liquid hydrogen target, and elastic $p+p$ differential cross sections were obtained over the angular range 6°–90° using CH and CH_2 targets. The quasielastic $\vec{p}+p$ data are in good agreement with existing elastic $\vec{p}+p$ data, suggesting that the effects of final state interactions and Fermi motion averaging are small at this energy for the range of momentum transfer covered by these data. Results of phase shift analyses are reported, and the amplitudes important to microscopic analysis of 800 MeV $\vec{p}+$nucleus elastic differential cross section and analyzing power data are discussed. Use of these amplitudes to generate the microscopic Kerman-McManus-Thaler optical potential for 800 MeV $\vec{p}+{}^{40}$Ca elastic scattering does not resolve the problems encountered previously concerning nuclear size information and poor fits to the analyzing power data.

NUCLEAR REACTIONS ^{2}H($\vec{p}$,pn)p, ^{2}H($\vec{p}$,pp)n, ^{1}H($\vec{p}$,p), ^{1}H(p,p); $E_{p,\text{inc}}$=800 MeV; measured $p+p$ elastic $d\sigma/d\Omega$ for $6° \leq \theta_{\text{c.m.}} \leq 90°$; measured $\vec{p}+p$ elastic $A_y(\theta)$ for $10° \leq \theta_{\text{c.m.}} \leq 47°$; measured $\vec{p}+p$ and $\vec{p}+n$ quasielastic $A_y(\theta)$ for $14° \leq \theta_{\text{c.m.}} \leq 75°$; CH, CH_2, liquid hydrogen and liquid deuterium targets; two arm coincidence for quasielastic; phase shift analyses; microscopic (KMT) optical model calculations for 800 MeV $\vec{p}+{}^{40}$Ca.

I. INTRODUCTION

The phenomenology of $\sim$1 GeV proton-nucleon (pN) scattering is of interest not only for studies of the nucleon-nucleon (NN) interaction and pionic inelasticities, but also because of the important role it plays in the microscopic analyses of $\sim$1 GeV proton-nucleus scattering data.[1–3]

Such proton-nucleus work uses theoretical models[4,5] which require, as input for numerical calculations, the pN scattering amplitudes appropriate for the nuclear medium; the momentum transfer components for $q \leq 2.0$ fm^{-1} are of particular importance to studies aimed at obtaining nuclear structure information. Most of the proton-nucleus analyses reported to date have assumed the validity of the impulse approximation (IA); under this assumption the required amplitudes are taken to be those characterizing the free pN interaction.[1–3]

Recently, however, a comparison of experimental $p+$ nucleus elastic data and parameter-free theoretical predictions showed that use of the free pN amplitudes fails to reproduce the data for momentum transfers $q \leq 0.75$ fm^{-1}, even at 800 MeV.[3] Preliminary work indicated that the 800 MeV *effective* pN spin-orbit amplitudes in the nuclear medium should

be larger than the free amplitudes by roughly 20–30% in the region of momentum transfers $q=0.5$ to 0.75 fm^{-1}, while a suppression (about 5%) of the spin-independent amplitudes was found to be required from $q=0$ to 0.75 fm^{-1}. One explanation for these observations is that the empirical amplitudes simulate important medium modifications of the free pN t matrix.[3]

Because the nuclear structure information deduced through analysis of the 800 MeV p + nucleus data and the appropriate pN amplitudes in the medium are intimately related, it is important to properly account for the effects of the nuclear medium. This in turn requires, as a starting point, *accurately determined* free pN amplitudes for the momentum transfer region germane to p+nucleus studies ($0 \leq q \leq 2.0$ fm^{-1}).

Recent experimental work[6–10] has provided considerable constraints on the proton-proton (pp) amplitudes at 800 MeV. An inspection of the nucleon-nucleon (NN) data base reveals, however, that high quality $p+p$ elastic differential cross section data do not exist for $q \geq 1$ fm^{-1} ($\theta_{\text{c.m.}} \geq 19°$). On the other hand, for the $p+n$ (or $n+p$) case, apart from differential cross section data,[11] there is little small-to-medium q data at energies near 800 MeV.

In this paper we present new 800 MeV $p+p$ elastic differential cross section ($d\sigma/d\Omega$) data ($6° \leq \theta_{\text{c.m.}} \leq 90°$) and quasielastic (deuterium target) $\vec{p}+n$ analyzing power [$A_y(\theta)$] data ($14° \leq \theta_{\text{c.m.}} \leq 75°$). Quasielastic and elastic $\vec{p}+p$ analyzing powers were also obtained during the experiment, and comparison of these data sets with previously obtained elastic $\vec{p}+p$ analyzing power data suggests that systematic uncertainties are small and that the elastic and quasielastic analyzing powers are the same (i.e., the effects of final state interactions and Fermi motion averaging are small at 800 MeV for the range of momentum transfer covered by these data). Thus, we believe that the new $\vec{p}+n$ quasielastic $A_y(\theta)$ data, as well as the $p+p$ elastic cross section data, improve the 800 MeV NN data base from which the elastic NN amplitudes are obtained through phase shift analysis.

Results of phase shift analyses of the NN data base including these new data are also reported. For both $p+p$ and $p+n$, we find that predictions obtained from fixed energy (750–843 MeV) and global (0–1 GeV) analyses are in basic agreement with each other and with the new, and most other existing, cross section and analyzing power data. The differences between the new spin-independent and spin-orbit amplitudes and the free amplitudes used in recent impulse-approximation analyses of p + nucleus scattering data are small, and do not resolve the problems encountered in the p+ nucleus work directed towards providing nuclear size information. We believe that the results of the present work significantly reduce the likelihood that inaccurate free pN amplitudes are the origin of the p + nucleus difficulties.

II. EXPERIMENTAL

A. General

Forward-angle elastic ($\vec{p}+p$, LH_2 target) and quasielastic ($\vec{p}+p$ and $\vec{p}+n$, LD_2 target) proton-nucleon analyzing power data, as well as elastic $p+p$ differential cross section data (CH and CH_2 targets), were obtained at the high resolution spectrometer (HRS) experimental area of the Los Alamos Clinton P. Anderson Meson Physics Facility (LAMPF). The data were obtained during LAMPF running cycles 24, 26, 29, 30 and 31. Beams of 800 MeV polarized ($\hat{n}$-type) and unpolarized protons were incident upon targets located at the center of the 1 m radius HRS scattering chamber. Two ion chambers (IC1 and IC2), located inside the scattering chamber about 0.75 m downstream of the target, were used to monitor the integrated beam current.

For the polarized beam runs, beam spin direction (up or down, perpendicular to the plane of scattering) was reversed at the ion source every 2–3 min, and a beam line polarimeter determined the average beam polarization for each run; beam polarization was typically 85%. Logic levels generated at the source were read by the HRS on-line data acquisition system to tag each recorded event according to beam polarization. In effect, for each target, two experiments were done simultaneously: one with beam polarization "up" and one with beam polarization "down". This technique eliminated most systematic sources of error from the calculated analyzing powers. For each HRS angle setting, the analyzing power was computed as

$$A_y(\theta)=\frac{1}{P_B}\frac{\sigma\uparrow-\sigma\downarrow}{\sigma\uparrow+\sigma\downarrow}\ , \tag{1}$$

where P_B is the beam polarization and $\sigma\uparrow$ and $\sigma\downarrow$ are the relative cross sections at angle θ when the beam spin direction is up and down, respectively.

For the coincidence measurements the HRS, described elsewhere,[12] detected the scattered forward-going proton (laboratory angles ranging from 6° to 33°), while a second arm, the recoil detection system, detected at conjugate laboratory angles (81° to 47°) recoil protons or neutrons in coincidence with protons detected by the HRS. The HRS momentum acceptance is $\simeq \pm 1\%$. The $p+p$ elastic differential cross section data were obtained using only the HRS (single arm experiment).

B. Cycle 24

The same 5 cm diam vertical cylindrical flask made of 0.13 mm thick Kapton was used for both LH_2 and LD_2. The recoil detection system consisted of a 5×5 array of plastic scintillators (Pilot B, dimensions of each, 7.5 cm$\times$7.5 cm$\times$15 cm), each optically coupled to EMI9813B photomultipliers. The array, mounted on an aluminum frame, was attached to the outside of the scattering chamber so that target-recoil detector distance was about 1 m. A thin (0.5 cm) plastic (Pilot B) scintillator (area of 40 cm$\times$40 cm), the charged particle detector, located between the target and the recoil array (also outside the scattering chamber) was used to tag recoil protons. This scintillator was coupled on two opposite ends to EMI9813B photomultipliers. The scattering chamber window between the target and the recoil array consisted of 0.5 cm thick plastic supported every 8 cm by 1 cm diam stainless steel rods. This experimental arrangement allowed simultaneous measurement of both quasielastic $\vec{p}+p$ and $\vec{p}+n$ analyzing powers (LD_2 target) for center-of-momentum scattering angles greater than 28°.

The data were obtained using the standard HRS data acquisition system with the addition of 26 TDC channels (CAMAC). Each event defined by the HRS focal plane scintillator system was used to start the series of time to digital converters (TDC's). The stops for 25 of these channels were taken from leading edge discriminators connected to each array counter photomultiplier. Neutron detection efficiency varied between 10—30% depending upon recoil energy. The discriminator outputs associated with the charged particle detector fed a meantimer which then provided a stop to the final TDC channel. In this way, the relative timing between events detected by the HRS and the recoil detection system was recorded.

Data were taped for every event defined by the standard HRS system (a fourfold coincidence among scintillators located on the focal plane), so that $\vec{p}+n$ and $\vec{p}+p$ data were obtained simultaneously. Depending upon the center-of-momentum scattering angle, the quasielastic peak occurred over 8 to 16 of the recoil counters; the yields from these counters were used in determining the quasielastic analyzing powers.

The initial system checkout was done using the LH_2 target. Data were obtained at laboratory scattering angles (HRS) of 5°, 7°, 9°, 11°, and 14° using only the HRS and at 17°, 18°, and 20° using both the HRS and the recoil detection system. Since accurate $\vec{p}+p$ $A_y(\theta)$ data were available[9,10] for comparison, these measurements provided a means of ensuring that the hardware and software necessary to determine the analyzing powers were operating properly. In addition, consistency checks were made at the angles where both single arm and coincidence data were obtained to ensure that the same calculated analyzing powers resulted.

The quasielastic (LD_2 target) analyzing power data were obtained at HRS laboratory angles 6° through 22° in 2° steps. At 6°, 8°, and 10° only $\vec{p}+n$ data could be obtained because the recoil protons were absorbed in the target and the scattering chamber window. An empty flask measurement was made at each angle so that flask generated contributions could be determined and subtracted from the flask full runs.

C. Cycle 26

A 3.8 cm diam vertical flask made of 0.08 mm thick Mylar was used for LD_2. The rest of the experimental setup was identical to that discussed in Sec. II B. Data were obtained for $\vec{p}+n$ and $\vec{p}+p$ at HRS angles of 18°, 20°, 22°, 24°, 26°, 28°, 31°, and 32.9°.

D. Cycle 29

The 3.8 cm flask was used for LD_2 and the single proton veto counter associated with the array assembly was replaced with four horizontal counters, each (0.5 cm thick) of area 40 cm$\times$10 cm (the recoil array was reconfigured to a 4×6 geometry to accommodate the new proton veto counters). These counters were optically coupled on each short edge to EMI9813B photomultipliers and the two discriminator outputs associated with each counter fed a meantimer. The four meantimer outputs were input to CAMAC TDC channels, and a software "or" was used to create a single TDC histogram for recoil protons.

Additional electronics were used to redefine events to be taped as either an HRS event *and* recoil neutron, *or* an HRS event *and* recoil proton; thus, for these runs, the $\vec{p}+n$ and $\vec{p}+p$ data were obtained serially.

Using this arrangement quasielastic data were obtained for laboratory scattering angles (HRS) of 10° and 15°. The coincidence requirement before taping data led to much improved statistical accuracy for these data as compared to that of the data obtained in cycles 24 and 26.

E. Cycle 30

The 800 MeV $p+p$ elastic differential cross section data were obtained using CH ($29.5\pm1\%$ mg/cm^2) and CH_2 ($67.9\pm1\%$ mg/cm^2 and $68.4\pm1\%$ mg/cm^2) targets. Data were obtained using the HRS at laboratory angles of 3.0°, 3.5°, 4.0°, 5.0°, 6.0°, 8.0°, 10.0°, 12.5°, 15.0°, 20.0°, 25.0°, 30.0°,

and 35.0°. The data for angles $< 15°$ were obtained using the CH target, while the data for angles $> 15°$ were obtained using the 67.9 mg/cm^2 CH_2 target. At angles 3.0°, 12.5°, and 15.0°, data were obtained using both the CH and 67.9 mg/cm^2 CH_2 targets to ensure proper relative normalization of the differential cross section obtained for each target. In addition, data were obtained at 35° (the last two runs) with both CH_2 targets to investigate hydrogen depletion in the 67.9 mg/cm^2 target which was used to obtain the 15°—35° data (no depletion was evident). During the course of the experiment, the ion chamber ratio IC1/IC2 remained constant to about 1.5%.

F. Cycle 31

The 3.8 cm diam flask was again used for LD_2, but the flask was offset in the horizontal (scattering) plane a distance of 1 cm in the direction perpendicular to the beam line (away from the recoil direction). A single neutron recoil array counter and an associated charged particle scintillator (Pilot B, 1 cm$\times$10 cm$\times$10 cm) were placed inside the scattering chamber at $\sim$90° to the beam line about 20 cm from the target. This arrangement made it possible to obtain both quasielastic $\vec{p}+n$ and $\vec{p}+p$ data at 6° laboratory (HRS) scattering angle ($\theta_{c.m.} = 14.3°$, corresponding to a recoil energy of about 12 MeV for the target nucleon initially at rest).

Following the 6° measurements, data were obtained at 30° (HRS) using the 24-counter array and associated four proton counters as discussed in Sec. II D. Both the 6° and 30° data were obtained by requiring either $p+p$ or $p+n$ coincidences before taping.

III. OFF-LINE ANALYSES AND RESULTS

A. Liquid hydrogen runs

Background-corrected yields were determined utilizing the empty flask data and the analyzing powers were computed using Eq. (1). The results are shown in Fig. 1, where they are compared with previous $\vec{p}+p$ analyzing power measurements and the results of the quasielastic measurements to be discussed. The curves shown in Fig. 1 are discussed in Sec. IV. The data are listed in Table I.

As seen in Fig. 1 and Table I, the $\vec{p}+p$ elastic data obtained with and without the recoil coincidence requirement are consistent to within experimental errors. These data are also in good agreement with the very precise (absolute errors typically < 0.01) data of Bevington *et al.*[9] and McNaughton

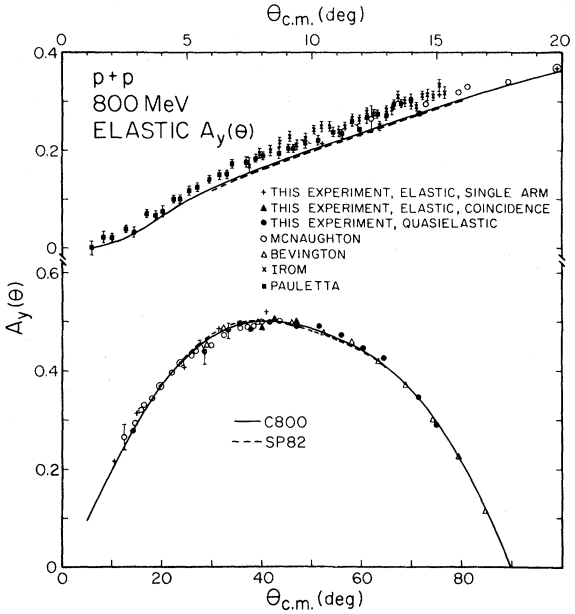

FIG. 1. The 800 MeV $\vec{p}+p$ elastic and quasielastic (deuterium target) analyzing power data obtained in this experiment are compared with other elastic data (Refs. 6, 7, 9, and 10). The curves are results of phase shift analyses discussed in the text.

et al.[10] in the region of overlap. Forward angle ($\theta_{c.m.} < 15°$) elastic data obtained by Irom *et al.*[6] and Pauletta *et al.*[7] are also seen (Fig. 1) to be consistent with the other data.

The off-line analysis of the LH_2 data enabled a determination of the proton detection efficiency of the thin 40 cm$\times$40 cm recoil counter. Although this information was not important in the determination of the elastic $\vec{p}+p$ analyzing powers, knowledge of the efficiency was *essential* for the quasielastic measurements, since failure to tag recoil protons leads to systematic errors in the quasielastic $\vec{p}+n$ analyzing powers. The efficiency was determined using the LH_2 data taken at HRS settings of 17° and 20° where the recoil system was used in coincidence with the HRS. The results indicated that the effective efficiency was 99.3% for tagging protons of energies from 95 to 125 MeV; we believe that the efficiency did not differ substantially over the range of recoil energies spanned by the quasielastic measurements that followed.

B. Liquid deuterium runs

For cycle 24 and 26 runs, where the $\vec{p}+p$ and $\vec{p}+n$ quasielastic data were obtained simultaneously, a software gate was placed on the peak in the proton counter TDC histogram (the time difference between the HRS trigger and the proton recoil

TABLE I. Elastic and quasielastic analyzing powers for *pp* and *pn* at 800 MeV.

		Quasielastic $\vec{p}n$ and $\vec{p}p$ analyzing powers				
θ_{lab} (deg)	$\theta_{c.m.}$ (deg)	A_y ($\vec{p}n$)	ΔA_y ($\vec{p}n$)	A_y ($\vec{p}p$)	ΔA_y ($\vec{p}p$)	Cycle
6	14.3	0.165	0.099			24
6	14.3	0.236	0.001	0.276	0.002	31
8	19.1	0.258	0.057			24
10	23.8	0.293	0.042			24
10	23.8	0.316	0.002	0.417	0.003	29
12	28.5	0.320	0.033	0.437	0.025	24
14	33.2	0.325	0.029	0.478	0.017	24
15	35.5	0.325	0.002	0.497	0.004	29
16	37.8	0.314	0.026	0.482	0.014	24
18	42.4	0.313	0.020	0.499	0.008	24,26
20	47.0	0.287	0.019	0.489	0.007	24,26
22	51.5	0.261	0.017	0.490	0.006	24,26
24	56.0	0.250	0.029	0.473	0.009	26
26	60.4	0.196	0.029	0.445	0.009	26
28	64.8	0.145	0.033	0.426	0.010	26
30	69.2	0.115	0.009			31
31	71.3	0.096	0.031	0.344	0.009	26
33	75.4	0.058	0.044	0.288	0.011	26
		Elastic $\vec{p}p$ analyzing powers				
θ_{lab} (deg)	$\theta_{c.m.}$ (deg)	A_y (HRS)	ΔA_y (HRS)	A_y (recoil)	ΔA_y (recoil)	Cycle
5	10.4	0.215	0.004			24
7	15.1	0.313	0.004			24
9	19.8	0.368	0.004			24
11	24.5	0.405	0.004			24
14	31.6	0.485	0.004			24
17	40.1	0.489	0.005	0.488	0.018	24
18	42.4	0.521	0.006	0.515	0.018	24
18	42.4	0.518	0.007	0.507	0.016	24
20	47.0	0.498	0.005	0.499	0.015	24

counter) to identify recoil protons. A typical histogram is shown in Fig. 2, where background contributions due to accidental coincidences are seen to be

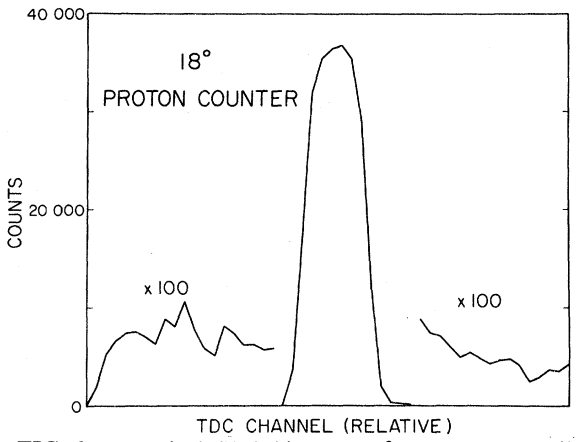

FIG. 2. A typical TDC histogram for the large recoil counter (proton tag) used to obtain the quasielastic (deuterium target) coincidence data.

≃0.2%. For cycle 29 and 31 runs, where the $\vec{p}+p$ and $\vec{p}+n$ data were obtained serially at each angle ($\vec{p}+p$ data obtained immediately following acquisition of the $\vec{p}+n$ data), the hardware event trigger definition provided crude recoil particle identification; a software gate on the four proton counter-TDC histogram was used to identify recoil protons.

For all runs, a software gate set on the missing mass (HRS) spectrum required that only quasielastic events were accepted. This gate was necessary at the most forward angles where both quasielastic (proton-nucleon) and proton-deuterium elastic events were detected by the HRS.

Multiple hit events (events in which more than one array detector triggered for a given HRS event) were eliminated during the off-line analysis. Two processes account for the majority of multiple hit events. The first occurs when a recoil particle directly or indirectly triggers two or more array counters. The other arises when a recoil particle triggers one array counter and a random particle

triggers another counter. Since it was not feasible to determine which of the triggered array counters registered the real time-correlated event, it was necessary to reject all multiple hit events in order to prevent double counting of an event. Multiple to single hit ratios varied, depending upon angle, between 5–15% for the $\vec{p}+p$ data and 5–25% for the $\vec{p}+n$ data. The elimination of multiple hit events typically lead to 1% ($\vec{p}+p$) and 3% ($\vec{p}+n$) corrections to the calculated analyzing powers.

Following the LD_2 and empty flask off-line analyses, the quasielastic proton and neutron yields for beam spins up and down were obtained. This was done by subtracting the least-squares fitted background (third order polynomial) from the region of the time-correlated peak. A typical TDC time-of-flight histogram for a neutron recoil counter is shown in Fig. 3. Because leading edge discriminators were used for the recoil counters, the neutron spectra were broader than the proton spectra due to the larger range of pulse heights seen by the recoil counters for recoil neutrons versus protons. Additional broadening for neutrons also occurs because the $n+p$ reactions leading to "detection" of neutrons occur over the full volume of each recoil counter. The background contribution to the time-correlated quasielastic $\vec{p}+n$ yield was typically $\leq 5\%$, and for quasielastic $\vec{p}+p$ the contribution was much less (0.2%). The background-corrected yields were then normalized for target full and target empty runs at each angle, and the coincidence yields for the LD_2 target were obtained. Target empty yields were typically a few percent of the target full yields. For cycle 24 and 26 data, it was assumed that 0.7% (99.3% proton efficiency for the 40 cm×40 cm proton recoil counter) of the protons

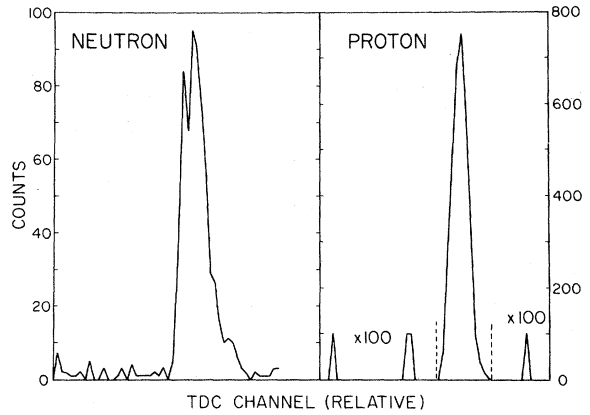

FIG. 3. Typical TDC histograms for one of the neutron array counters used in the quasielastic (deuterium) coincidence experiment. The FWHM of the neutron peak is approximately 3 ns.

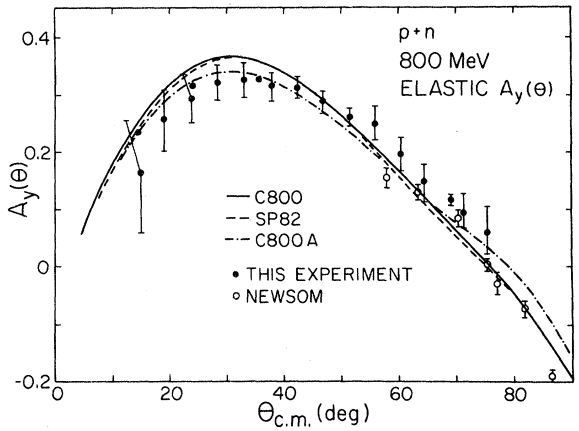

FIG. 4. The $\vec{p}+n$ quasielastic (deuterium) analyzing power data obtained in this experiment are compared with those of Newsom (Ref. 13) and with the results of phase shift analyses discussed in the text.

were misidentified as neutrons; the measured neutron yields were corrected based on this assumption. The improved geometry and smaller proton recoil counters (four 10 cm×40 cm scintillators) used during cycles 29 and 31 led to an estimated > 99.9% efficiency for proton identification, and no corrections to neutron yields were made for these data. Finally, Eq. (1) was used to calculate the analyzing powers.

The resulting quasielastic $\vec{p}+p$ analyzing powers are shown in Fig. 1 while the quasielastic $\vec{p}+n$ analyzing powers are shown in Fig. 4. The errors shown reflect statistical and background subtraction contributions only. Numerical values are given in Table I. The curves are discussed in Sec. IV. The center-of-momentum scattering angle, $\theta_{c.m.}$, was determined from elastic nucleon-nucleon kinematics at 800 MeV for the HRS angle corresponding to maximum yield. The HRS angular acceptance in the plane of scattering is about ±1°.

The $\vec{p}+p$ quasielastic data (Fig. 1) are seen to be in good agreement with the elastic data. This is evidence that effects of final state interactions and Fermi motion averaging are small over the region of momentum transfer covered by the quasielastic data (see Sec. V).

As seen in Fig. 4 and Table I, the statistical and background subtraction errors associated with the $\vec{p}+n$ quasielastic data are typically 0.02–0.03 for cycle 24 and 26 data and < 0.01 for cycle 29 and 31 data. Also shown in Fig. 4 are some of the elastic $n+\vec{p}$ data obtained by Newsom.[13] The two data sets are in reasonable agreement over the region of overlap. Because the $\vec{p}+n$ quasielastic data were obtained simultaneously with $\vec{p}+p$ quasielastic data, and because the $\vec{p}+p$ quasielastic data are in

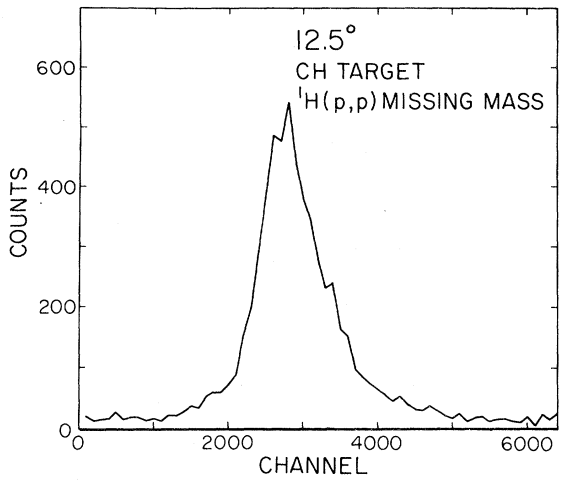

FIG. 5. The ^{1}H(p,p) missing mass spectrum obtained at 12.5° (lab) using a CH target. The horizontal scale is such that the FWHM of the peak is about 900 keV.

excellent agreement with very accurate elastic (see Fig. 1) $\vec{p}+p$ data,[9,10] we believe the systematic absolute normalization uncertainty of the new data presented in Fig. 4 to be small (see Sec. III D).

C. CH and CH_2 runs

The differential cross section data were sorted into $\simeq 0.3°$ angular bins. The ^{1}H(p,p) missing mass spectrum for each angle (except for laboratory angles $\leq 6°$) contained a narrow (FWHM < 0.9 MeV) $p+p$ elastic "line" and a small, relatively flat background due primarily to quasielastic scattering from the ^{12}C in the CH or CH_2 target. For each angle the background under the elastic peak was determined and subtracted to obtain the relative $p+p$ differential cross section. This background contribution was usually about 5%. A typical missing mass spectrum is shown in Fig. 5. For each laboratory angle less than 6°, there was no quasielastic contribution to the ^{1}H(p,p) missing mass spectrum, but it did contain yields from ^{12}C(p,p') to the first few excited states. When these yields "crossed" the $p+p$ elastic region, they were appropriately determined and subtracted.

The HRS system consists of a beam line dispersion matched to a quadrupole-dipole-dipole spectrometer which operates in the "momentum-loss" mode.[12] The scattering and dispersion planes are orthogonal, such that the focal-plane position perpendicular to the dispersion axis is proportional to the scattering angle in the reaction plane. For ^{1}H(p,p) elastic scattering at 800 MeV, the kinematical $dE/d\theta$ of the scattered protons (θ is the scattering angle) is large, becoming about 14 MeV/deg at 35 deg laboratory. Since the focal plane is about 30 MeV wide (for 800 MeV protons), and since the HRS acceptance in the plane of scattering is about $\pm 1°$, the elastic protons from ^{1}H(p,p) can occupy (in the dispersion direction) the entire focal plane. It is therefore important to account for the changes in relative efficiency across the focal plane. This efficiency was measured by sweeping a ^{208}Pb(p,p) elastic "line" (where $dE/d\theta$ is small) across the focal plane by varying the HRS fields; five such relative efficiency measurements were made at equal intervals across the focal plane. It was observed that the extreme variations in relative efficiency were about $\pm 6\%$. This information was used in the relative normalization of the ^{1}H(p,p) data.

The absolute normalization of the cross section data was obtained in the region $14° \leq \theta_{\text{c.m.}} \leq 16°$ by cross normalizing to the data of Irom *et al.*[6] (absolute normalization $\pm 3\%$). In this angular range the Irom data are in basic agreement with the Andreev *et al.*[8] data (absolute normalization $\pm 5\%$). However, at smaller angles the Irom and Andreev data differ by as much as 10%. We also obtained a relative normalization to the $p+^{208}$Pb elastic data obtained during the focal plane mapping, and a cross normalization to the data of Ref. 14 (absolute normalization $\pm 5\%$) yielded an absolute normalization consistent with that obtained from the Irom data.

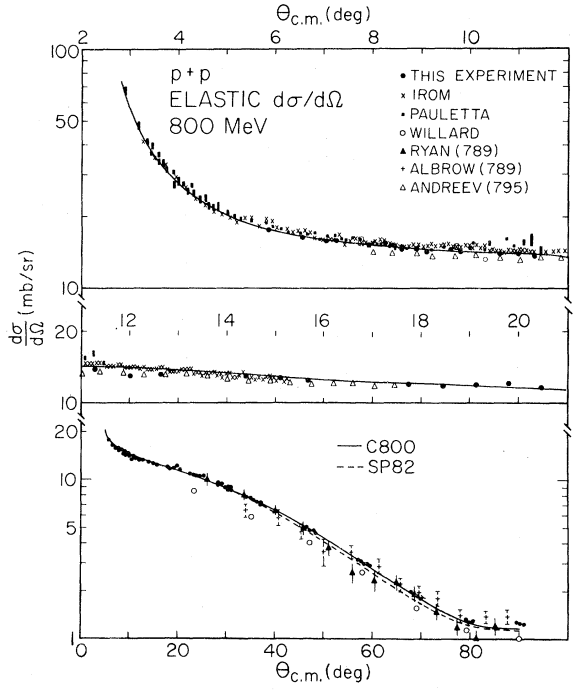

FIG. 6. The $p+p$ elastic differential cross section data obtained in this experiment are compared to other data sets (Refs. 6, 8, 15, and 17) and to the results of phase shift analyses discussed in the text.

TABLE II. Differential cross sections for $^1H(p,p)$ at 800 MeV.

$\theta_{c.m.}$ (deg)	$d\sigma/d\Omega$ (mb/sr)	$\theta_{c.m.}$ (deg)	$d\sigma/d\Omega$ (mb/sr)
5.86	17.67±0.5	29.06	9.21±0.14
6.55	16.26±0.5	29.73	8.84±0.16
7.06	15.70±0.4	29.73	8.87±0.14
7.23	15.79±0.5	30.40	8.91±0.16
7.74	15.79±0.4	30.40	8.61±0.14
7.91	15.23±0.5	31.07	8.89±0.16
8.25	15.41±0.3	31.07	8.51±0.13
8.42	15.04±0.4	34.23	7.69±0.11
8.60	14.38±0.5	34.89	7.64±0.12
8.93	14.95±0.3	34.89	7.59±0.11
9.11	14.00±0.4	35.56	7.32±0.12
9.62	14.47±0.3	35.56	7.26±0.11
9.79	14.00±0.4	36.23	7.15±0.11
10.30	13.16±0.3	36.23	7.24±0.12
10.63	13.82±0.3	36.89	6.92±0.12
10.98	13.91±0.3	36.89	7.15±0.11
11.32	13.54±0.3	45.75	5.09±0.07
12.00	12.88±0.3	46.40	4.98±0.07
12.68	12.88±0.3	47.05	4.67±0.06
14.38	12.97±0.2	47.70	4.66±0.07
15.06	12.60±0.2	48.35	4.55±0.07
15.74	12.22±0.2	57.02	3.07±0.04
17.77	11.94±0.2	57.65	3.09±0.04
18.45	11.75±0.2	58.30	2.90±0.04
19.12	11.84±0.2	58.93	2.92±0.04
19.80	12.13±0.2	59.56	2.84±0.04
20.48	11.56±0.2	68.62	1.95±0.02
22.50	10.90±0.2	69.24	1.81±0.02
23.18	10.72±0.2	69.85	1.79±0.02
23.85	10.62±0.2	79.27	1.34±0.02
24.53	10.43±0.2	79.87	1.29±0.02
25.20	10.53±0.2	80.47	1.29±0.02
28.38	9.19±0.16	89.52	1.18±0.01
28.38	9.40±0.10	90.10	1.15±0.01
29.06	9.30±0.16	90.68	1.13±0.01

The renormalization factors for phase shift solution C800 (see Sec. IV) are 0.99, 0.97, and 1.03, for the new, Irom, and Andreev data, respectively. Based upon the various consistencies and the quoted absolute errors associated with the Irom and Andreev data, we believe uncertainty in the absolute normalization of the data presented here to be $\leq \pm 5\%$. The data are shown in Fig. 6, along with other data[6–8,15–17] and with phase shift predictions to be discussed in Sec. IV. The data are tabulated in Table II. The errors shown reflect statistical and background contributions only, and vary between 1% and 4%. Apart from the obvious normalization discrepancy between the Willard[17] data and the other data sets, there is generally very good agreement between the various overlapping data sets spanning the entire $3° \leq \theta_{c.m.} \leq 90°$ region.

D. Systematic uncertainties

The errors associated with the analyzing powers determined using the coincidence techniques (Table I) reflect not only the statistical uncertainties of the measurements, but also account for the uncertainty in the determination of the background under each of the peaks in the TDC histograms and the statistical uncertainty in the determination of the average beam polarization. In addition, certain systematic uncertainties may exist which are not reflected in the error bars quoted.

One source of systematic error results from uncertainties in the relative integrated beam currents for the two beam polarization states. This error is quite small ($<$ 1% for the worst case) since the primary and backup beam current monitors (ion chambers)

tracked to 1.5% during the course of the experiment.

Another source of systematic error is the failure to properly identify the type of recoil particle detected by the array counters. Since both recoil neutrons and protons are detected by the array counters, false asymmetries may be introduced into the results if the quasielastic $\vec{p}+p$ and $\vec{p}+n$ analyzing powers differ and misidentifications of recoil particles occur. Only recoil events which were time-correlated with the HRS events were accepted in the determination of the yields used in the computation of the analyzing powers. Thus, the main mechanisms for recoil particle misidentification were the proton veto counter failing to trigger for a recoil proton or the veto counter triggering on a recoil neutron. The latter leads to negligible error because of a combination of the small detection efficiency of this counter for neutrons and the relatively small detection efficiency (roughly 10—30 %) of the array counters for neutrons. The former could be significant due to the large efficiency ($\simeq$100%) of the array counters for protons which are not tagged by the proton recoil counter. For cycle 24 and 26 data this effect was taken into account by assuming that 0.7% of the neutron yield originated from misidentified protons (the proton veto counter efficiency was measured to be 99.3%). The differences between corrected and uncorrected analyzing powers were strongly dependent upon angle because of the different angular dependences of the $\vec{p}+p$ and $\vec{p}+n$ analyzing powers. Typically the corrected $\vec{p}+n$ $A_y(\theta)$ was smaller than the uncorrected $A_y(\theta)$ by 0—5 % for $14° < \theta_{\text{c.m.}} < 47°$, by 5—15% for $47° < \theta_{\text{c.m.}} < 65°$, and by 15—30 % for $65° < \theta_{\text{c.m.}} < 75°$. The proton veto counter efficiency was taken to be 100% for cycles 29 and 31 because of the much improved geometry of this counter.

Systematic errors may also be introduced into the results during the analysis of the data. The elimination of all multiple hits in the off-line analysis is one source of such an error. As mentioned in Sec. III B the elimination of multiple hits typically led to 1% ($\vec{p}+p$) and 3% ($\vec{p}+n$) corrections to the calculated analyzing powers. Eliminating events in which a random coincidence was involved could lead to a false asymmetry if the beam currents were significantly different in the two beam polarization states. However, beam current monitor ratios, as well as ratios of single hits to multiple hits in the recoil array, indicated that the beam current did not vary significantly between the two beam polarization states. This source of systematic error is therefore quite small ($\ll$ 1%).

Another source of systematic error for the analyzing power experiment is the absolute calibration of the beam line polarimeter. This calibration by itself could add an overall ±2—3 % uncertainty to the analyzing power data. However, actual systematic uncertainties are probably $\simeq$1—2 % for the measured $A_y(\theta)$ since the $\vec{p}+p$ data obtained in this experiment agree at this level with the data of Bevington and McNaughton.[9,10] We believe the absolute normalization of Bevington-McNaughton (+ 1%, −0.5%) to be reliable and quite accurate because of the considerable care that went into the determination using the quench ratio technique. Changes in beam phase space and changes in the angle of incidence of the beam on target, with polarization reversal, have been studied in detail during previous polarized beam experiments[18] using the HRS and were found to have a negligible effect on the measured analyzing powers. Figure 7 shows, on an expanded vertical scale for the 30°—60° region, the good agreement at the 1% level among the various data sets for $\vec{p}+p$ $A_y(\theta)$ at 800 MeV. In this figure the error bars on the Bevington-McNaughton data[9,10] include the systematic uncertainties (+ 1.0%, −0.5%). Finally, the focal plane position relative efficiency determination associated with the $p+p$ elastic data leads to an additional $\sim\pm$1—3 % uncertainty to be associated with each data point for $\theta_{\text{lab}} > 10°$.

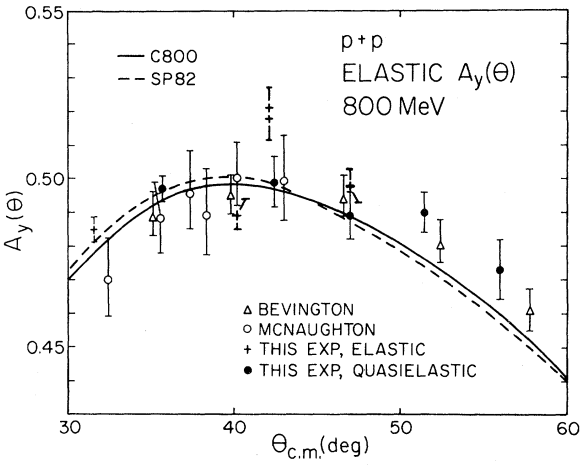

FIG. 7. For the $30° \leq \theta_{\text{c.m.}} \leq 60°$ region some of the data of Fig. 1 are shown in an expanded vertical scale to emphasize the good agreement among the various data sets at the percent level. The error bars on the Bevington-McNaughton data include systematic uncertainties (+1.0%, −0.5%).

IV. PHASE SHIFT ANALYSES

The new 800 MeV $p+p$ elastic differential cross section and $\vec{p}+n$ quasielastic analyzing power data (deuterium target) were added to the nucleon-

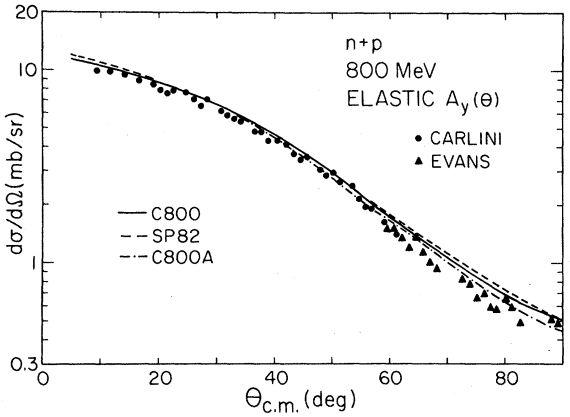

FIG. 8. The 800 MeV $n+p$ elastic differential cross section data of Refs. 11 and 20 are compared to the results of the phase shift analyses discussed in the text.

nucleon (NN) data base of the phase shift analysis program SAID, and new solutions C800 and SP82 were generated incorporating these data.[19] C800 is a fixed energy solution which uses NN data from 750 to 843 MeV to generate phase shifts over this energy range; with the addition of the data presented in this paper the C800 solution was generated from 655 and 341 pp and np data points, respectively. SP82 is a global solution for 0–1 GeV, and including the data presented here, used 5207 and 5283 pp and np data points, respectively.

The solid curves shown in Figs. 1, 4, 6, and 7 are C800 results, while the dashed curves are SP82 results. Shown in Fig. 8 are the available 800 MeV $n+p$ differential cross section data[11,20] for $\theta_{c.m.} \leq 90°$ and the C800 and SP82 solutions. The solid and dashed curves of Fig. 9 correspond to the C800 and SP82 phase shift fits to the total and total reaction cross sections. Also shown in Fig. 9 are the experimental data[21] and theoretical constraints[22] (shown as data points) used in the analyses. As seen from these figures, there is little difference between the observables predicted by C800 and SP82, and the overall agreement with the experimental data is quite good.

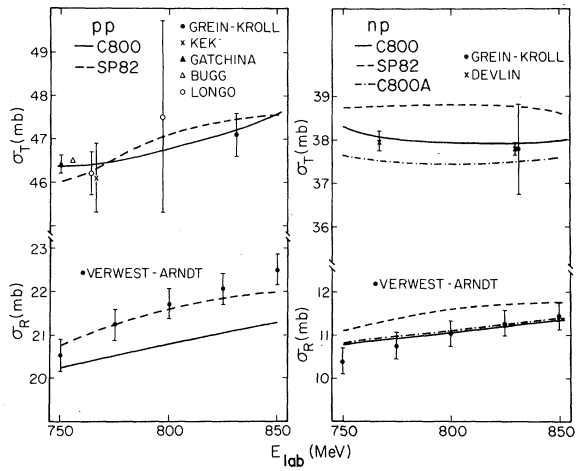

FIG. 9. The predictions for total and reaction cross sections of the phase shift solutions discussed in the text are compared to the experimental data (Ref. 21) and theoretical constraints (Ref. 22).

As seen in Fig. 1, the $\vec{p}+p$ analyzing power obtained from either phase shift analysis reproduces quite well the overall magnitude and shape of the experimental data, although the data appear to be systematically larger (about 10%) than the phase shift results for center-of-momentum angles less than 16°. Since the overall systematic error assigned to the Irom[6] and Pauletta[7] data is $\simeq$5%, and since these data sets are in basic agreement with the McNaughton data near 16°, the discrepancy needs further investigation. The C800 and SP82 phase shift results for the $\vec{p}+n$ analyzing power (Fig. 4) are in good agreement with the data, apart from a slight systematic normalization discrepancy of about 7%.

The phase shift predictions for the $p+p$ elastic differential cross section (Fig. 6) also follow quite closely the trend of the data. However, systematic differences (at the 10% level) exist for the various data sets which span the 8° to 13° region. For angles greater than 20° it is evident that the normalization and overall slope of the Willard[17] data are systematically different from those of the remaining data sets. Good agreement is also seen in Fig. 8 between the available $n+p$ elastic differential cross section data and the C800 and SP82 results for angles $10° \leq \theta_{c.m.} \leq 60°$. At the larger angles the phase shift results are systematically higher than the data by roughly 15%.

It is informative to determine whether more accurate $p+n$ data would significantly affect the outcome of the phase shift analyses. An option of SAID[19] was utilized to greatly enhance the sensitivity of the C800 solution to the data shown in Figs. 4 and 8. Only the $I=0$ phases were varied so that the $I=1$ components of the C800 solution remained unchanged. The new solution, C800A, is depicted by the dot-dashed curves in Figs. 4, 8, and 9. Some visual improvement is observed in the fits to both the cross section and analyzing power data. The $|\chi|^2$ per $p+n$ datum of solution C800 is 2.3 (total $|\chi|^2$ of 793 for 341 datum), while a value of 2.9 was obtained for solution C800A. An examination of the $|\chi|^2$ values for the 28 sets of $n+p$ data used by C800 revealed that the only significant discrepancy between the C800 and C800A solutions is for the spin-transfer quantities[23] K_{NN} and K_{SS} at large an-

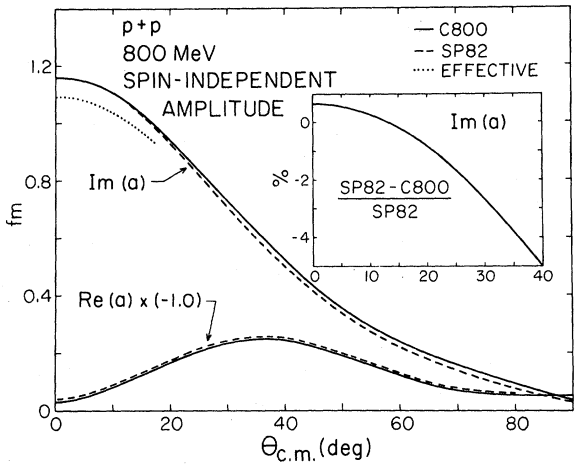

FIG. 10. The spin-independent amplitudes of phase shift solutions C800 and SP82 for 800 MeV $p+p$. See text for discussion of effective amplitude. The insert shows, for Im(a), the percent difference between the SP82 and C800 solutions.

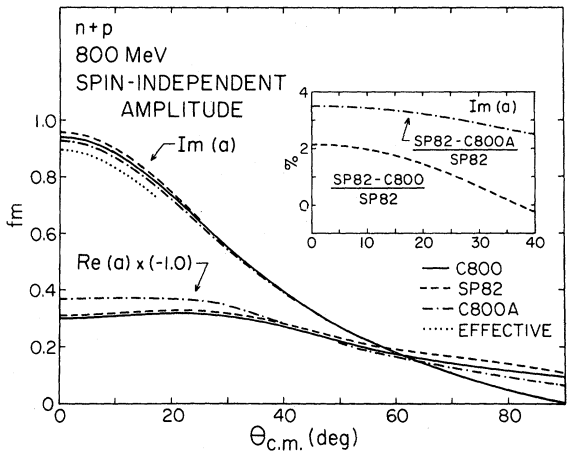

FIG. 12. The spin-independent amplitudes of phase shift solutions C800, SP82, and C800A for 800 MeV $p+n$. See text for discussion of effective amplitude. The insert has the same meaning as in Fig. 10.

gles ($\theta_{c.m.} > 160°$), where the $|\chi|^2$ per datum increases by factors from 3 to 5.

Shown in Figs. 10—13 are the spin-independent [$a(q)$] and spin-orbit [$c(q)$] amplitudes[24] which resulted from the various phase shift analyses discussed above. Figures 14 and 15 show the resulting uncertainties associated with the C800 solution. Thus, Figs. 10—15 can be taken to suggest the present level at which these amplitudes are determined for proton-nucleon scattering at 800 MeV. In particular, the Im(a) and Im(c) components, required for the microscopic analyses of 800 MeV $p+$ nucleus elastic cross section and analyzing power data, appear to be determined at the level of a few percent for center-of-momentum scattering angles less than 40° ($q \leq 2$ fm^{-1}). The uncertainties in the other components are typically $\leq 5\%$ for $q \leq 2$ fm^{-1}, except for Re(a_{pp}) which has a larger uncertainty at small q. The dotted curves of Figs. 10—13 indicate the effective amplitudes used in Ref. 3 to obtain the expected ^{40}Ca neutron-proton root-mean-square radius difference of -0.05 fm and an improved description of the analyzing power through microscopic analysis of 800 MeV $\vec{p}+^{40}$Ca elastic data.

We note, however, that a complete amplitude determination at 800 MeV requires 9 (11) independent measurements for $p+p$ ($p+n$) spanning the re-

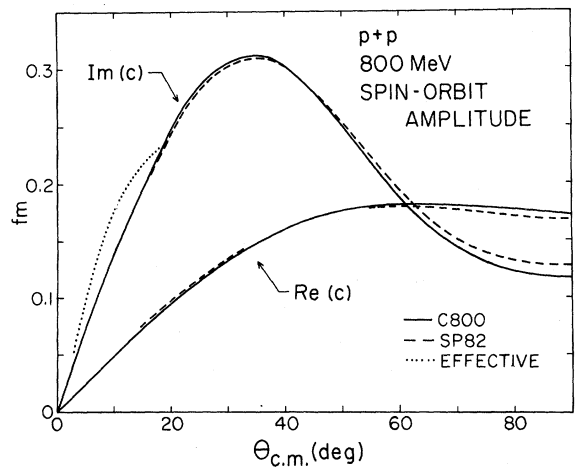

FIG. 11. The spin-dependent amplitudes of phase shift solutions C800 and SP82 for 800 MeV $\vec{p}+p$. See text for discussion of effective amplitude.

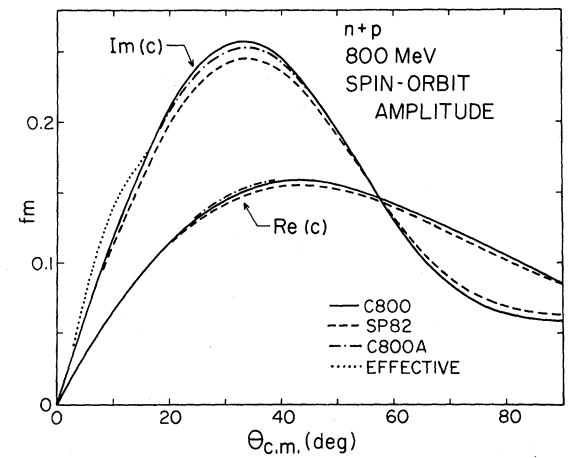

FIG. 13. The spin-dependent amplitudes of phase shift solutions C800, SP82, and C800A for 800 MeV $\vec{p}+n$. See text for discussion of effective amplitude.

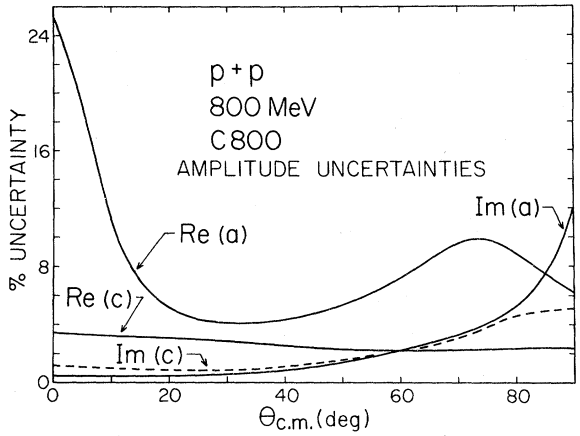

FIG. 14. The uncertainties of the 800 MeV $p+p$ spin-independent and spin-dependent amplitudes of phase shift solution C800.

gion of momentum transfer for which the amplitudes are to be determined. For the *pp* case a sufficient number of experiments have been performed over a broad enough range of momentum transfer that the *pp* solution is fairly well determined[10]; additional $p+p$ data will only lead to improved accuracy. On the other hand, an insufficient number of $p+n$ (or $n+p$) experiments have been performed at energies near 800 MeV to allow the conclusion that the *pn* solution is unique. To remedy this situation, we have recently initiated an experimental program to measure some of the 800 MeV $p+n$ depolarization parameters for small to medium momentum transfer. We comment here that some of the preliminary data (e.g., D_{SS} and D_{LL}) are not even in qualitative agreement with any of the phase shift solutions discussed above. We also note that a preliminary attempt was made to obtain a phase shift solution consistent with these data and to determine the changes to be anticipated in the spin-independent $[a(q)]$ and spin-dependent $[c(q)]$ amplitudes (compared to the C800 and SP82 results) when the double-spin-flip amplitudes are realistically constrained. Roughly speaking, our preliminary investigation indicates that changes of about 10% for $a(q)$ and $c(q)$ can be expected for the *pn* channel.

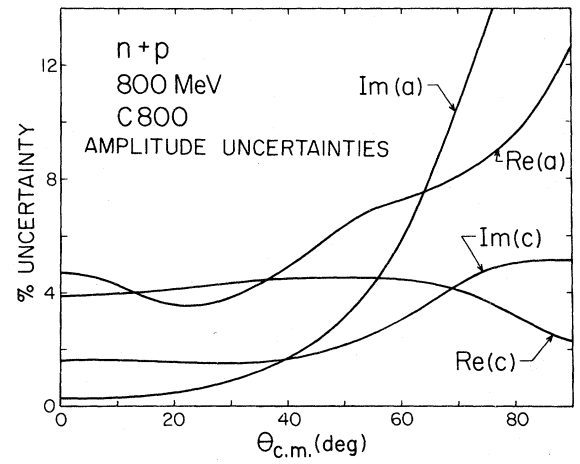

FIG. 15. The uncertainties of the 800 MeV $p+n$ spin-independent and spin-dependent amplitudes of phase shift solution C800.

We also caution that the amplitude uncertainties associated with the phase shift analyses under discussion are characteristic of these particular phase shift analyses. The amplitude uncertainties are influenced not only by the data base, but also by other constraints built into the analyses and the specific approach taken in the analyses. Thus, other phase shift analyses may give results different from those shown in Figs. 10—15. In particular, the Bystricky-Lechanoine-Lehar[25] phase shift analysis gives a $\mathrm{Re}[a_{pn}]$ near 800 MeV which is significantly different from the amplitude shown in Fig. 12. We have not investigated the origin of this discrepancy.

V. COMMENTS ON FINAL STATE INTERACTIONS AND FERMI MOTION AVERAGING

As mentioned earlier, we have interpreted the experimental equality of the free and quasifree (deuterium target) $\vec{p}+p$ analyzing powers to mean that final state interactions and Fermi motion averaging do not result in quasielastic analyzing powers for $\vec{p}+N$ that are different from the free values (at the percent level) for the range of momentum transfer covered by the quasielastic data. There is also theoretical support for our experimental observations. Harrington[26] has considered the effects of the final state interactions associated with using deuterium as a neutron target and has concluded that such effects are only at the few percent level for momentum transfers above 100 MeV/*c*; the smallest momentum transfer associated with our quasielastic data set is 150 MeV/*c*.

The possible effects of Fermi motion averaging are interesting and deserve additional comment. Taking the Fermi momentum of the deuteron as 45 MeV/*c*, and using the total invariant energy, we find that 800 MeV proton + nucleon quasielastic scattering from the nucleons in deuterium samples, in the extreme limit, the proton-nucleon interaction from 732 to 872 MeV with a mean energy of 806 MeV (laboratory equivalent incident energies for target nucleon initially at rest). For a given beam energy and spectrometer field and angle setting the Mandelstam variable t associated with a given data point is fixed, regardless of the total pN energy. We there-

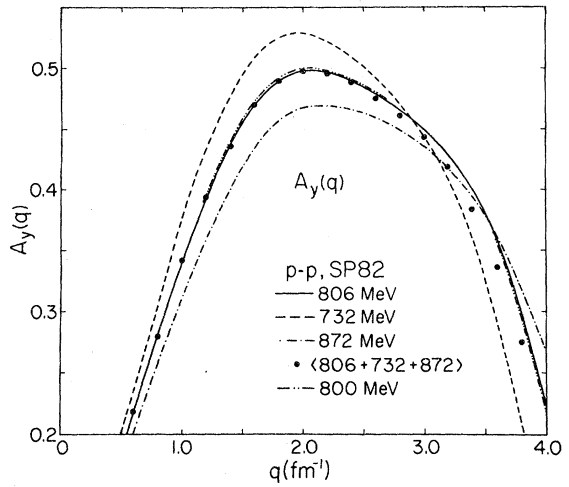

FIG. 16. The curves are the SP82 predictions for the $\vec{p}+p$ analyzing powers at 732, 800, 806, and 872 MeV (see text). The dots represent the average of the 806, 732, and 872 MeV values.

fore plotted, in Figs. 16 and 17, the SP82 predictions for $\vec{p}+N$ analyzing powers at the above extreme laboratory equivalent energies as a function of momentum transfer. The energy dependence of the analyzing powers is evident for both systems, but the nature of this dependence is such that the appropriate average over energies (at the same momentum transfer) is very nearly the value obtained for the incident beam energy as if the target nucleons were at rest. The large dots in Figs. 16 and 17 are the simple average of the 732, 806, and 872 MeV curves. When this averaging is done more carefully, the result will be in even better agreement with the 806 MeV values. As seen in Figs. 16 and 17, the 800 MeV curves are basically equivalent to the 806 MeV curves. This situation is fortuitous and due to

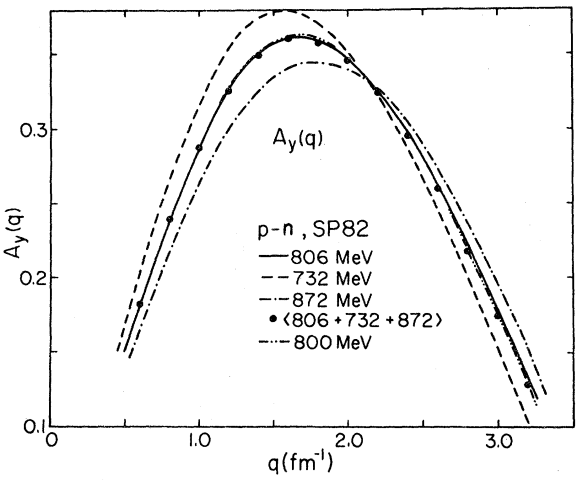

FIG. 17. Same as Fig. 16, except 800 MeV $\vec{p}+n$.

the fact that, at a given momentum transfer, $A_y(\theta)$ for both $\vec{p}+p$ and $\vec{p}+n$ is nearly a linear function of energy from 732 to 872 MeV. Based on Figs. 16 and 17, we conclude that the effects of Fermi motion averaging contribute to departures of the measured analyzing powers (quasielastic, deuterium) from the free values by magnitudes much less than 0.01 at 800 MeV.

VI. ANALYSIS OF 800 MeV $\vec{p}$ + NUCLEUS ELASTIC DATA

In the past, conventional theoretical descriptions of medium energy p +nucleus elastic scattering have invoked the impulse approximation within the framework of the microscopic optical potential formalism of Kerman-McManus-Thaler (KMT) or the Glauber multiple scattering formalism.[1-5] Validity of the impulse approximation implies that the appropriate amplitudes for the calculations are those describing the free pN scattering; for the case of a spin-zero target nucleus, only the spin-independent $[a(q)]$ and spin-orbit $[c(q)]$ amplitudes are required in first order.

However, supposed uncertainty in the small-to-medium q behavior of these fundamental amplitudes was claimed to be justification for using empirical amplitudes which lead to better predictions for the $p+$ nucleus observables,[1,2] although more recently[3] it has been suggested that important medium modifications to the small-to-medium momentum transfer components of these amplitudes are necessarily required (dotted curves in Figs. 10—13). Thus, it is important to determine if the new and more accurate phase shift (free) amplitudes are sufficiently constrained to support this conclusion. Section IV indicates the uncertainties that presently exist in the determination of the spin-independent and spin-orbit amplitudes.

Second-order KMT calculations were made for 800 MeV $\vec{p}+^{40}$Ca elastic scattering using the three sets of amplitudes discussed in Sec. IV. Details of the theoretical calculations may be found in Refs. 1 and 2. As with past calculations,[1-3] the point-proton density was obtained from the accurate empirical charge density, while the point-neutron density was assumed to be characterized by a three-parameter Fermi distribution, and the parameters were varied to obtain a best fit to the differential cross section data.

Excellent (and equivalent) fits to the 800 MeV $\vec{p}+^{40}$Ca elastic angular distribution data[1] were obtained using either of the SP82, C800, or C800A amplitudes. Each of these fits is comparable to that shown in Fig. 1 of Ref. 1. The deduced neutron-proton root-mean-square (rms) radius differences for

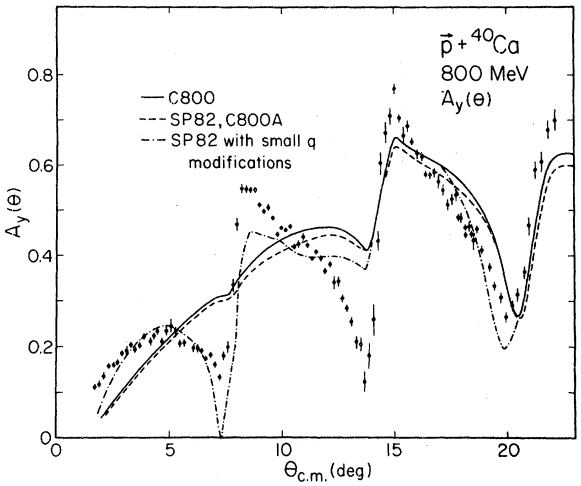

FIG. 18. The 800 MeV $\vec{p}+{}^{40}$Ca analyzing power data (Ref. 27) are compared to results of KMT optical model calculations obtained using the three phase shift solutions discussed in the text. The dot-dashed curve is the result of a KMT calculation using an empirically modified SP82 amplitude (see text).

^{40}Ca are found to be $\Delta r_{np}=-0.18$, -0.16, and -0.14 fm when using the SP82, C800, and C800A amplitudes, respectively. Extensive error analyses done in the past[2] have indicated, assuming the model to be correct, that an additional uncertainty of ± 0.05 fm should be assigned to these results. Thus, the present results indicate that the deduced Δr_{np} for ^{40}Ca is -0.16 ± 0.07 fm, in disagreement, as noted in Ref. 1, with theoretical expectations (-0.05 fm) by about -0.1 fm.

Figure 18 compares the 800 MeV $\vec{p}+{}^{40}$Ca analyzing power data[27] with the predictions obtained using the SP82, C800, and C800A amplitudes. The failure of these calculations to reproduce the structure in the data at small angles is evident. The situation is much the same as that encountered earlier[1] when using amplitudes determined from earlier phase shift analyses. Finally, a KMT calculation was made using the SP82 amplitudes with the same small q modifications discussed in Ref. 3 (see the dotted curves in Figs. 10 and 11). Again an excellent fit to the differential cross section was obtained, but in this instance the deduced neutron-proton rms radius difference was found to be -0.08 fm, and an improved description of the analyzing power was obtained (see the dot-dashed curve of Fig. 18). We emphasize that for this calculation the small q modifications were not optimized to give a better fit to the $A_y(\theta)$ data; they were taken as specified in Ref. 3 to simply illustrate the dramatic changes in the predicted $A_y(\theta)$ that result with inclusion of such modifications. Finally, we note that the modified amplitudes are well outside the error corridors associated with the free amplitudes. Thus, use of more accurate free amplitudes does not change the conclusions reached previously[3] concerning breakdown of the impulse approximation at small momentum transfers and the need for a careful study of the effects of the nuclear medium.

VII. SUMMARY AND CONCLUSIONS

We have obtained and presented, new, small-to-medium momentum transfer, $p+p$ elastic cross section data, and $\vec{p}+n$ quasielastic (deuterium target) analyzing power data. During the course of the experiment we also obtained free and quasielastic (deuterium) $\vec{p}+p$ analyzing power data. The free and quasielastic $\vec{p}+p$ data sets are in agreement with each other and with previously measured free $\vec{p}+p$ analyzing power data, suggesting that the effects of final state interactions and Fermi motion averaging are small at 800 MeV for the range of momentum transfer covered by these new data. Other arguments were given as to why we expect the free and quasielastic results to be the same.

With the addition of the new data presented here, for both $p+p$ and $p+n$ (or $n+p$), a sufficient amount of high quality differential cross section and analyzing power data now exists for the small-to-medium momentum transfer region ($\theta_{\text{c.m.}}\leq 90°$) to provide stringent constraints on phase shift analyses in this momentum transfer region. The results of phase shift analyses were also reported. Both fixed energy (750–843 MeV) and global (0–1 GeV) phase shift solutions were obtained and found to give results which are consistent with the data base and with each other. We calculated, however, that changes in the phase shift solutions for the $p+n$ channel are expected when accurate $p+n$ triple scattering data become available. Using the KMT formalism we performed microscopic optical model analyses of 800 MeV $\vec{p}+{}^{40}$Ca elastic cross section and analyzing power data using the new amplitudes and did not obtain the expected nuclear matter radius or reproduce the trends of the analyzing power data. Finally, we reinforce our earlier conclusions that the proton-nucleus impulse approximation work most likely suffers from the omission of medium modifications to the free amplitudes over the momentum transfer region $q\leq 1$–2 fm^{-1} rather than from inaccurately determined free amplitudes from the phase shift analyses.

This work was supported in part by the U.S. Department of Energy and The Robert A. Welch Foundation.

*Present address: Department of Physics, Rutgers University, New Brunswick, NJ 08903.

[1]L. Ray *et al.*, Phys Rev. C 23, 828 (1981).
[2]L. Ray, W. R. Coker, and G. W. Hoffmann, Phys. Rev. C 18, 2641 (1978).
[3]G. W. Hoffmann *et al.*, Phys. Rev. Lett. 47, 1436 (1981).
[4]A. K. Kerman, H. McManus, and R. M. Thaler, Ann. Phys. (N.Y.) 8, 551 (1959).
[5]R. J. Glauber, in *Lectures in Theoretical Physics,* edited by W. E. Brittin and L. G. Dunham (Interscience, New York, 1959), pp. 315–413.
[6]F. Irom, G. J. Igo, J. B. McClelland, and C. A. Whitten, Jr., Phys. Rev. C 25, 373 (1982).
[7]A. Wriekat *et al.*, Phys. Lett. 97B, 33 (1980); G. Pauletta *et al.* (unpublished).
[8]V. A. Andreev *et al.*, Gatchina Report No. 656, 1981 (unpublished).
[9]P. R. Bevington *et al.*, Phys. Rev. Lett. 41, 384 (1978).
[10]M. W. McNaughton *et al.*, Phys. Rev. C 23, 1128 (1981); 25, 1967 (1982).
[11]R. Carlini *et al.*, Phys. Rev. Lett. 41, 1341 (1978).
[12]B. Ziedman, Los Alamos National Laboratory Report LA-4773-MS, 1971 (unpublished), part 1.
[13]C. Newsom, Ph.D. thesis, The University of Texas at Austin, 1980 (unpublished).
[14]G. W. Hoffmann *et al.*, Phys. Rev. C 21, 1488 (1980).
[15]B. A. Ryan *et al.*, Phys. Rev. D 3, 1 (1971).
[16]M. G. Albrow *et al.*, Nucl. Phys. B23, 445 (1970).
[17]H. B. Willard *et al.*, Phys. Rev. C 14, 1545 (1976).
[18]G. W. Hoffmann *et al.*, Phys. Rev. Lett. 40, 1256 (1978).
[19]R. A. Arndt and D. Roper, Virginia Polytechnic Institute and State University, Scattering Analysis Interactive Dialin (SAID).
[20]M. L. Evans *et al.*, Phys. Rev. Lett. 36, 497 (1976).
[21]G. N. Valichko *et al.*, Gatchina Report No. 655, 1981 (unpublished); S. S. Yamamoto, private communication; D. V. Bugg *et al.*, Phys. Rev. 146, 980 (1966); M. J. Longo and B. J. Meyer, *ibid.* 125, 701 (1962); M. J. Longo *et al.*, Phys. Rev. Lett. 3, 568 (1959); T. J. Devlin *et al.*, Phys. Rev. D 8, 136 (1973).
[22]W. Grein and P. Kroll, SIN Report PR-81-09; B. J. VerWest and R. A. Arndt, Phys. Rev. C 25, 1979 (1982).
[23]R. D. Ransome *et al.*, Phys. Rev. Lett. 48, 781 (1982).
[24]M. H. MacGregor, M. J. Moravcsik, and H. P. Stapp, Annu. Rev. Nucl. Sci. 10, 291 (1960).
[25]J. Bystricky, C. Lechanoine, and F. Lehar, Saclay Report D Ph P E 79-01, 1979.
[26]D. R. Harrington, in *High Energy Physics and Nuclear Structure, Proceedings of the Fifth International Conference, Uppsala, 1973,* edited by G. Tibell (North-Holland, Amsterdam, 1974), pp. 118–122.
[27]G. Igo *et al.*, Phys. Lett. 81B, 151 (1979).